Thermal transport in a two-dimensional $\mathbb{Z}_2$ spin liquid

Alexandros Metavitsiadis,[1,*] Angelo Pidatella,[2,†] and Wolfram Brenig[1,‡]
[1]*Institute for Theoretical Physics, Technical University Braunschweig, D-38106 Braunschweig, Germany*
[2]*Institute for Theoretical Physics, Technical University Dresden, D-01062 Dresden, Germany*
(Received 18 July 2017; revised manuscript received 24 October 2017; published 13 November 2017)

We study the dynamical thermal conductivity of the two-dimensional Kitaev spin model on the honeycomb lattice. We find a strongly temperature dependent low-frequency spectral intensity as a direct consequence of fractionalization of spins into mobile Majorana matter and a static $\mathbb{Z}_2$ gauge field. The latter acts as an emergent thermally activated disorder, leading to the appearance of a pseudogap which closes in the thermodynamic limit, indicating a dissipative heat conductor. Our analysis is based on complementary calculations of the current correlation function, comprising exact diagonalization by means of a complete summation over all gauge sectors, as well as a phenomenological mean-field treatment of thermal gauge fluctuations, valid at intermediate and high temperatures. The results will also be contrasted against the conductivity discarding gauge fluctuations.

DOI: 10.1103/PhysRevB.96.205121

I. INTRODUCTION

Thermal transport is an important tool to study elementary magnetic excitations in local moment materials. This has been demonstrated in a large variety of systems displaying excitations, which range from conventional spin waves to exotic fractional quasiparticles, including magnons [1–8], triplons [9,10], spinons [11–16], and emergent magnetic monopoles [17–20]. Most recently, the first thermal transport measurements have appeared in systems with strong spin-orbit coupling (SOC), which are potentially proximate to 2D spin-liquid states [21–23].

Quantum magnets with SOC have attracted considerable interest, because they allow for directionally dependent highly anisotropic superexchange, which can lead to strongly frustrated quantum magnets [24–27]. Among them is Kitaev's model on the honeycomb lattice [28]. It constitutes the rare case of a 2D spin system with an exactly known spin-liquid ground state and fractionalization of spins in terms of bulk Majorana fermions and $\mathbb{Z}_2$ gauge fields [28–32]. Part of its quantum phases are perturbatively equivalent to the toric code [33], providing a direct link to paradigmatic models of topological order [34,35]. In finite magnetic fields the $\mathbb{Z}_2$ vortices acquire non-Abelian anyonic statistics and the Majorana Dirac spectrum opens a gap displaying a chiral edge mode [28].

There is an ongoing quest for Kitaev materials with 2D honeycomb variants Na_2IrO_3 [36], α-Li_2IrO_3 [37], α-$RuCl_3$ [38], and 3D polymorphs β-,γ-Li_2IrO_3 [39,40], as well as triangular lattice versions $Ba_3IrTi_2O_9$ under scrutiny [41]. Presently, all compounds show significant non-Kitaev exchange. The role of coupling to extrinsic degrees of freedom, such as phonons, is an open issue [23]. In pursuit of signatures of fractionalization, an enormous amount of research has been performed on the spin dynamics in Kitaev models and materials, including the dynamic structure factor [42–44], Raman scattering [45,46], and nuclear magnetic resonance [47]. Thermal conductivity measurements on α-$RuCl_3$ [21–23] have mostly been confined to the longitudinal component κ_{xx} and reveal [23] that the heat transport seems intimately related to spin-phonon coupling. Very recently, observations of putative chiral edge modes [28], using off-diagonal κ_{xy} at finite magnetic fields, have appeared in literature [48].

Theoretically, fractionalization has long been a topic for magnetic transport in 1D quantum magnets, due to the existence of spinons in Heisenberg chains and dimerized or frustrated variants thereof [49,50]. One key question is the dissipation of currents, which has been investigated extensively at zero frequency (dc) and momentum in connection with the linear response Drude weight (DW) [51–57], which is the nondissipating dc part of the current autocorrelation function and, if existent, indicates a ballistic channel of the fractional quasiparticles.

First theoretical studies of heat transport in Kitaev models have been carried out on chains [58] and ladders [59] with very different conclusions. In the former, gauge fields are absent and the chain is found to be a perfect, ballistic heat conductor with a finite thermal DW. The ladder is the simplest quasi-1D descendant of the honeycomb lattice model featuring both matter fermions and $\mathbb{Z}_2$ gauge fields. It is found to display no ballistic channel and a zero frequency insulating pseudogap. This is a direct consequence of fractionalization, with the static gauge fields acting as an emergent, thermally induced disorder, which scatters the current carrying mobile Majorana matter. Since dimensionality of the Majorana matter could have a significant impact on the scattering from the gauge field, the prime motivation of the present work is to extend the ideas of Ref. [59] to 2D. As our central results, we find that similar to Ref. [59], ballistic channels are suppressed and finite low-frequency spectral weight is generated in the dynamical conductivity by scattering from the gauge field. However, in sharp contrast to the ladder, the pseudogap does not survive the thermodynamic limit in 2D, leading to a dissipative heat conductor, rather than an insulator.

The paper is organized as follows. In Sec. II, we provide details of the Kitaev model as needed for this work. In Sec. III we summarize magnetic heat transport theory in the linear response regime. In Sec. IV we present and compare our results, derived from three complementary methods, i.e., exact diagonalization (ED), Sec. IV A, average gauge configuration

*a.metavitsiadis@tu-bs.de
†angelo.pidatella@tu-dresden.de
‡w.brenig@tu-bs.de

(AGC) calculations, Sec. IV B, and zero vortex sector (ZVS) analytic evaluations, Sec. IV C. Lastly, Sec. V contains our conclusions.

II. KITAEV MODEL

In this section we briefly summarize several points, clarifying the use of Kitaev's model [28] in this work. The Hamiltonian reads

$$H = \sum_{\langle l,m\rangle,\alpha(\langle l,m\rangle)} J_\alpha \sigma_l^\alpha \sigma_m^\alpha , \tag{1}$$

where $\langle l,m\rangle$ refer to the sites on the nearest neighbor bonds of the honeycomb lattice. For simplicity, in this paper, we will envisage the honeycomb lattice to be deformed into the so-called brickwall lattice (BWL) [29,30], shown in Fig. 1. J_α and σ^α are the exchange coupling constants and Pauli matrices, respectively, for coordinates $\alpha = x,y,z$. The relation $\alpha(\langle l,m\rangle)$ can be read off from the red, green, and blue bond coloring in Fig. 1. It is known that this model can be mapped onto free spinless ('matter') fermions in the presence of static $\mathbb{Z}_2$ gauge fluxes. The allowed values ± 1 of the latter are related to the eigenvalues of the conserved operator $\Phi = \prod_{l=1\ldots6} \sigma_l^{\alpha(l)}$ around each plaquette, Fig. 1, where $\alpha(l) = x,y,z$, refers to that component of the exchange link which is *not* part of the loop passing site l [28]. For the remainder of this paper we set $\hbar$, k_B, and the lattice constant a to unity, and choose J_z as the unit of energy.

Several routes have been established to map the spins in Eq. (1) to fermions, e.g., using overcomplete sets of Majorana fermions [28], Jordan-Wigner transformation [29,30], or bond

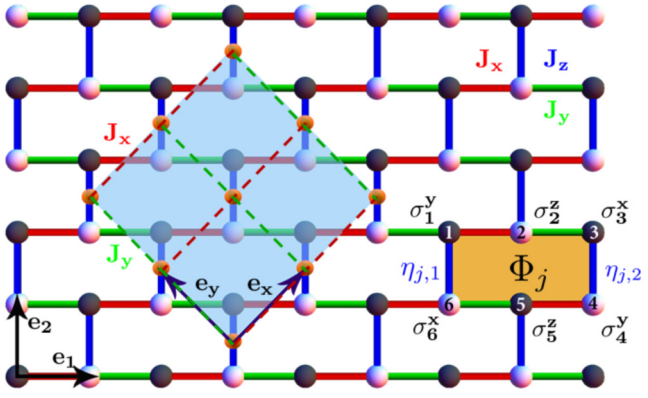

FIG. 1. Kitaev model on a honeycomb lattice, deformed into the so-called brickwall lattice. The J_x, J_y, and J_z exchange links are indicated by red, green, and blue lines, respectively, and the two sublattices with dark and light color bullets. The lattice is formed along the $\mathbf{e}_1$, $\mathbf{e}_2$ directions. The dark yellowish bullets lying on the middle of the z links indicate the vertices of the effective square lattice (ESL), rotated to the left by 45°, with unit vectors $\mathbf{e}_x$, $\mathbf{e}_y$ (light blue shaded region). The exchange interactions for the ESL are J_x and J_y along the $\mathbf{e}_x$ and $\mathbf{e}_y$ directions, respectively. The flux operator Φ_j of the jth plaquette is the product of the six spin operators around the plaquette, as shown in the dark yellowish highlighted region. The eigenvalue of the flux operator on that plaquette is equal to the product of the two corresponding η fields belonging to the same plaquette, i.e., $\Phi_j = \prod_{l=1}^6 \sigma_{jl}^{\alpha(l)} = \eta_{j,1}\eta_{j,2}$.

algebras [31]. While intermediate steps of these mappings are rather distinct, eventually all arrive at the same bulk Hamiltonian. On a BWL lattice of $2N$ sites, it comprises $2N$ free Majorana fermions—dubbed *mobile Majorana matter* in the literature—in the presence of N static $\mathbb{Z}_2$ gauge field variables residing on the z bonds. By introducing one spinless complex fermion for each pair of Majorana fermions on each z bond of the BWL the resulting final Hamiltonian reads [30]

$$H = \sum_{\mathbf{r}} h(\mathbf{r}) , \tag{2}$$

with $h(\mathbf{r})$ the single particle local energy

$$\begin{aligned} h(\mathbf{r}) = {} & J_x(d_{\mathbf{r}}^\dagger + d_{\mathbf{r}})(d_{\mathbf{r}+\mathbf{e}_x}^\dagger - d_{\mathbf{r}+\mathbf{e}_x}) + J_y(d_{\mathbf{r}}^\dagger + d_{\mathbf{r}}) \\ & \times (d_{\mathbf{r}+\mathbf{e}_y}^\dagger - d_{\mathbf{r}+\mathbf{e}_y}) + J_z\eta_{\mathbf{r}}(2d_{\mathbf{r}}^\dagger d_{\mathbf{r}} - 1) . \end{aligned} \tag{3}$$

$d_{\mathbf{r}}^{(\dagger)}$ and $\eta_{\mathbf{r}} = \pm 1$ refer to the spinless matter fermions and the gauge fields, which can be visualized to be located on the sites of a dual lattice of the z bonds of the BWL, forming an effective square lattice (ESL) of N sites, Fig. 1. In the fermionic representation $\Phi_{\mathbf{r}} = \eta_{\mathbf{r}}\eta_{\mathbf{r}+\mathbf{e}_1}$, for the brickwall lattice, and $\Phi_{\mathbf{r}} = \eta_{\mathbf{r}}\eta_{\mathbf{r}+\mathbf{e}_x-\mathbf{e}_y}$ for the ESL. From the preceding, it is rather apparent that the ESL model lacks C_4 symmetry and the two diagonal directions $\mathbf{e}_x \pm \mathbf{e}_y$ are distinct.

While the focus of our paper is on bulk transport properties, we state three remarks of caution regarding boundary conditions. First, the mapping from Eq. (1) is exact only if periodic boundary conditions (PBCs) are used along the $\mathbf{e}_2$ direction of the BWL [29,30]. Requiring PBCs also along the x,y chains ($\mathbf{e}_1$ direction of the BWL), requires consideration of surface terms [30,32], as known from any Jordan-Wigner type of mapping. It has been shown recently that for bulk thermal transport on Kitaev ladders such surface terms have no relevant effect [59], and therefore we discard them. Second, to describe bulk properties based on the ESL, it is natural to apply PBCs along the $\mathbf{e}_{x,y}$ directions of the lattice. This implies nonstandard $O(1/L)$ finite size corrections for a system of $N = L \times L$ sites. We do not expect these to be of any qualitative relevance. Third, and finally, the spectrum of the Kitaev model is highly degenerate. The relevance of this for the current correlation function is briefly commented on in Appendix A.

III. THERMAL TRANSPORT

The primary goal of this paper is to evaluate the dynamical equilibrium *bulk* thermal conductivity of the Kitaev model. In this section, and for completeness, we recollect the basic ingredients for this.

To start, linear response theory [60] with respect to a real space dependent local equilibrium temperature $T + \delta T(\mathbf{r})$ has to be performed, based on a canonical density matrix $\rho = \exp[-\int d^3r\,(\beta + \delta\beta(r))h(\mathbf{r})]$, where $\beta = 1/T$, and $h(\mathbf{r})$ is a local energy density which has to fulfill $H = \int d^3r\, h(\mathbf{r})$, where H is the Hamiltonian. In this framework, the linearized expectation value of the μ component of the energy current $\mathcal{J}_\mu$ in d dimensions is obtained from the dynamical thermal conductivity tensor $\kappa_{\mu\nu}(\mathbf{q},\omega)$ at wave vector $\mathbf{q}$ and frequency

ω through

$$\langle \mathcal{J}_\mu(\mathbf{q},\omega)\rangle = \sum_{\nu=1}^{d} \kappa_{\mu\nu}(\mathbf{q},\omega)\partial_\nu T(\mathbf{q},\omega)\,. \tag{4}$$

The equilibrium thermal expectation value $\langle A\rangle$ reads $\langle A\rangle = \mathrm{Tr}Ae^{-\beta H}/Z$, with $Z = \mathrm{Tr}e^{-\beta H}$ the partition function. The spectrum $\kappa'_{\mu\nu}(\omega)$, namely the real part of the thermal conductivity, follows from the Fourier transform of the current correlation function, $C_{\mu\nu}(\omega)$,

$$\kappa'_{\mu\nu}(\omega) = \frac{\beta}{2\omega}(1-e^{-\beta\omega})\,C_{\mu\nu}(\omega), \tag{5}$$

$$C_{\mu\nu}(\omega) = \int dt e^{i\omega t} C_{\mu\nu}(t),\; C_{\mu\nu}(t) = \frac{1}{N}\,\langle \mathcal{J}_\mu(t)\mathcal{J}_\nu\rangle. \tag{6}$$

It is customary to decompose $C_{\mu\nu}(\omega)$ as [49]

$$C_{\mu\nu}(\omega) = 4\pi\, D_{\mu\nu} T^2\,\delta(\omega) + C^{reg}_{\mu\nu}(\omega)\,, \tag{7}$$

where the *regular* part refers to $C^{reg}_{\mu\nu}(\omega) = C_{\mu\nu}(\omega\neq 0)$ and the *Drude* weight (DW) $D_{\mu\nu}$ is a measure for the ballistic contribution to the heat flow

$$D_{\mu\nu} = \frac{\beta^2}{2ZV}\sum_{E_l=E_m} e^{-\beta E_l}\langle l|\mathcal{J}_\mu|m\rangle\langle m|\mathcal{J}_\nu|l\rangle\,. \tag{8}$$

Because of Eq. (5), $\kappa'_{\mu\nu}(\omega) = 2\pi\, D_{\mu\nu}\delta(\omega) + \kappa^{reg}_{\mu\nu}(\omega)$. Whenever $D_{\mu\nu}\neq 0$, the system is a perfect heat conductor in channel $\mu\nu$. Otherwise it is a dissipative conductor with a limiting dc heat conductivity of $\kappa^{dc}_{\mu\nu} = \kappa'_{\mu\nu}(\omega\to 0)$. If both, $D_{\mu\nu}=0$ and $\kappa^{dc}_{\mu\nu}=0$, the system is an insulator in channel $\mu\nu$.

To determine the energy current $\mathcal{J}$ we turn to a real space version of the continuity equation $\partial_t h(\mathbf{r}) + \nabla\cdot\mathcal{J}(\mathbf{r}) = 0$, which is more amenable to describe the spinless fermions of Hamiltonian (2) and (3), which comprise a real space dependent potential by virtue of $\eta_{\mathbf{r}}$. To this end we use the polarization operator $\mathbf{P}$ [59],

$$\mathcal{J} = i[H,\mathbf{P}], \quad \text{with} \quad \mathbf{P} = \sum_{\mathbf{r}} \mathbf{r}\, h(\mathbf{r})\,, \tag{9}$$

which yields the same current operator as the continuity equation in the limit of $\mathbf{q}\to 0$ for a homogeneous system. For the Kitaev model on the ESL and using our *definition* of the energy density, given in Eq. (3), we arrive at the energy current

$$\mathcal{J}_\mu = 2i\,J_\mu \sum_{\mathbf{r}} [J_z\eta_{\mathbf{r}} b_{\mathbf{r}} b_{\mathbf{r}-\mathbf{e}_\mu} + \tau_\mu J_{\bar\mu} b_{\mathbf{r}} b_{\mathbf{r}+\mathbf{e}_x-\mathbf{e}_y}], \tag{10}$$

where $b_{\mathbf{r}} = (d^\dagger_{\mathbf{r}} + d_{\mathbf{r}})$, $\bar\mu = y(x)$, and $\tau_\mu = +(-)$ for $\mu = x(y)$. From the expression above, one can readily see that also the energy current operator is diagonal in the gauge fields.

We caution that the only requirement for $h(\mathbf{r})$ is that $H = \int d^3r\, h(\mathbf{r})$. This may be a reason for differing *quantitative* results for the Drude weight and the regular conductivity spectrum, obtained in recent studies of various frustrated and spin ladder models [55,58,60–63]. However, it is generally believed that universal *qualitative* statements, concerning the existence or absence of finite Drude weights and dc conductivities are insensitive to the freedom of choice for the energy density.

IV. EVALUATION OF HEAT CURRENT CORRELATION FUNCTIONS

Even though Kitaev's model comprises free fermions, the distribution of the $\eta_{\mathbf{r}}$ in real space renders analytical evaluation of thermal traces infeasible. Numerically, quantum Monte-Carlo (QMC) methods have been used for a variety of observables [63–66]. Regarding thermal transport, to the best of our knowledge, exact diagonalization (ED) [59], summing over all gauge configurations, supplemented also by approximate methods, has been used first to evaluate $C_{\mu\mu}(t)$ for the Kitaev Hamiltonian on a ladder [59]. Here we will extend this work to $d=2$ dimensions. In 2D, $C_{xy}(t)$, the off diagonal thermal transport coefficient may also be of interest, in particular in the non-Abelian phase at finite magnetic fields [28]. Here chiral edge states could give rise to quantized values of κ_{xy}—describing a thermal Hall conductivity—for temperatures well below the gap which is opened by the magnetic field [28,48]. In this paper we will not consider finite magnetic fields and analyze the *longitudinal* heat transport properties, i.e., $C_{\mu\mu}$, $\kappa'_{\mu\mu}$, and $D_{\mu\mu}$, at finite temperatures, using unbiased exact diagonalization, as well as an approximate ensemble of average gauge configurations. In addition, we perform an illustrative evaluation of $C_{\mu\mu}(\omega)$, and $D_{\mu\mu}(T)$ based on only the uniform gauge.

For the remainder of the paper, the dynamical transport properties are presented via the correlation function $C_{\mu\mu}(\omega,T)$ while regarding the experimentally relevant static transport properties, we present the DW $D_{\mu\mu}(T)$ and the dc thermal conductivity $\kappa^{dc}_{\mu\mu}(T)$. We focus on the isotropic gapless point $J_x = J_y = J_z$ unless mentioned otherwise.

A. Exact diagonalization (ED)

Since the energy current operator is diagonal in the gauge field, the correlation function $C_{\mu\mu}(t)$ can be written as

$$C_{\mu\mu}(t) = \frac{1}{ZN} Tr_\eta[Z_{d(\eta)}\,\langle \mathcal{J}_\mu(t)\mathcal{J}_\mu\rangle_{d(\eta)}]\,, \tag{11}$$

where N is the number of lattice sites of the ESL, the subscript $d(\eta)$ refers to tracing over matter fermions at a *fixed* gauge field state and the subsectors' partition functions $Z_{d(\eta)}$ sum up to the total partition function Z. To numerically evaluate Eq. (11), we resort to ED. To this end, we define a $2N$ component operator $\mathbf{D}^\dagger = (d^\dagger_1,\ldots,d^\dagger_N,d_1,\ldots,d_N)$ of the matter fermions. The indices $\{1,2,\ldots,N\}$ label all sites $\mathbf{r}$ of the ESL. In terms of $\mathbf{D}^\dagger$ the Hamiltonian and the current are set up in real space as $H = \mathbf{D}^\dagger\mathbf{h}(\eta)\mathbf{D}$, and $\mathcal{J}_\mu = \mathbf{D}^\dagger\mathbf{j}_\mu(\eta)\mathbf{D}$. Both $\mathbf{h}(\eta)$ and $\mathbf{j}_\mu(\eta)$ are $2N\times 2N$ matrices, which depend on the actual state of the gauge field $\eta = (\eta_1,\eta_2,\ldots,\eta_N)$. For each given η we compute a Bogoliubov transformation $\mathbf{U}$, which introduces canonical quasiparticle fermions $\mathbf{A}^\dagger = (a^\dagger_1,\ldots,a^\dagger_N,a_1,\ldots,a_N)$ via $\mathbf{A} = \mathbf{U}^\dagger\mathbf{D}$ and maps the Hamiltonian to $H = \frac{1}{2}\mathbf{A}^\dagger\mathbf{E}\mathbf{A}$, where $\mathbf{E}$ is diagonal and $\mathrm{diag}(E) = (\varepsilon_1,\ldots,\varepsilon_N,-\varepsilon_1,\ldots,-\varepsilon_N)$, with ε_j being the quasiparticle energies.

With these definitions, the current correlation function in a fixed gauge configuration reads

$$C^\eta_{\mu\mu}(\omega) = \frac{2\pi}{N}\sum_{klmn} L_{kl}L_{mn}(\langle A^\dagger_k A_n\rangle\langle A_l A^\dagger_m\rangle - \langle A^\dagger_k A^\dagger_m\rangle\langle A_l A_n\rangle)\delta(\varepsilon_l-\varepsilon_k-\omega)\,, \tag{12}$$

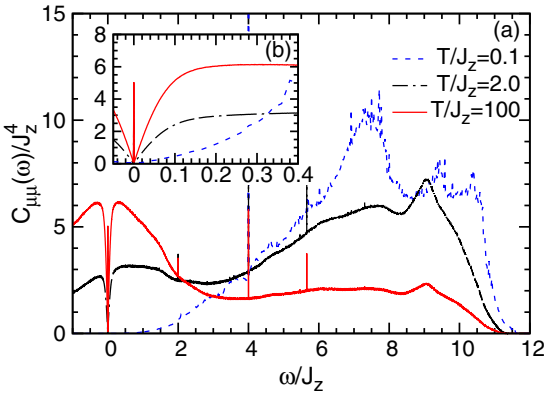

FIG. 2. (a) $C_{\mu\mu}(\omega)$ obtained by ED for a lattice of $N = 6 \times 6$ sites at three different temperatures $T/J_z = 0.1, 2, 100$. (b) Low frequency zoom of (a).

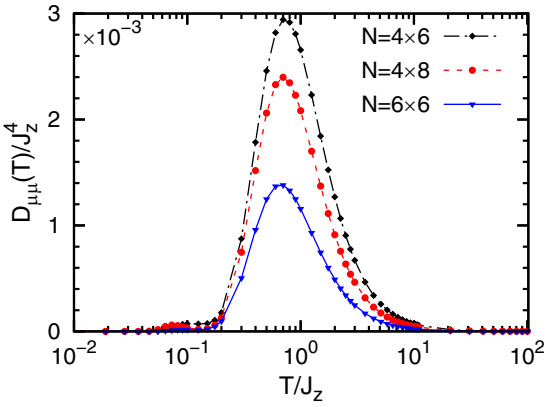

FIG. 3. Drude weight $D_{\mu\mu}(T)$ versus temperature for three different system sizes obtained via ED.

where $\mathbf{L} = \mathbf{U}^\dagger \mathbf{j}(\eta)\mathbf{U}$ and $\langle A_\mu^{(\dagger)} A_\nu^{(\dagger)} \rangle$ is either zero, f_j, or $(1 - f_j)$, depending on the components of the spinor $\mathbf{A}$ involved, and $f_j = 1/(e^{\beta\varepsilon_j} + 1)$ is the Fermi-Dirac distribution. Since the partition functions $Z_{d(\eta)}$ are byproducts of the ED for each gauge subsector, tracing the latter and Eq. (9), as in Eq. (11) completes the evaluation of $C_{\mu\mu}(\omega)$.

In Fig. 2, we present the frequency dependence of the correlation function $C_{\mu\mu}(\omega)$ for three temperatures $T/J_z = 0.1, 2, 100$. We note that we focus only on the positive frequency spectrum, $\omega > 0$, because $C_{\mu\mu}(-\omega) = e^{-\beta\omega} C_{\mu\mu}(\omega)$, as required by detailed balance. To reduce the computational effort for the evaluation of full traces over the 2^N possible gauge field configurations, we make use of translation symmetry. This allows us to reach systems up to $N = 36$ sites corresponding to an enormous Hilbert space dimension of the underlying spin model of 2^{72} states. The δ functions are binned in windows of $\delta\omega = 10^{-3}$, except for the lowest temperature, $T/J_z = 0.1$, at which a binning of $\delta\omega = 0.02$ has been chosen due to the larger finite size effects. The sharp peaks at finite frequencies are amplified by the very fine binning, and they are not expected to survive in the thermodynamic limit.

Equation (12) allows for two types of spectral contributions, namely quasiparticle, i.e., $\varepsilon_l \varepsilon_k > 0$, or pairbreaking, i.e., $\varepsilon_l \varepsilon_k < 0$, transport. The high frequency spectral weight $(\omega/J_z \gtrsim 6)$ in Fig. 2 is solely generated by the pairbreaking terms, and it is only quantitatively affected by the gauge excitations. Contrarily, the quasiparticle contribution is related to the matter fermion density relaxation and therefore is strongly affected by scattering from the gauge fields. As is obvious from Fig. 2, the latter contribution displays a weight strongly increasing with T which directly reflects the temperature dependence of the matter fermion occupation number. As shown in Sec. IV C, assuming only the ground state gauge, the complete quasiparticle transport accumulates into only a single T-dependent DW. In the presence of randomly distributed gauge excitation however, i.e., taking into account that the majority of gauge sectors lacks translational invariance, most of the DW spreads over a finite low-ω range, in a nonmonotonous way, exhibiting also a prominent low frequency depletion. Hence, for all temperatures $T/J_z \gtrsim 1$ the spectrum is *qualitatively* different from that discarding gauge excitations, Sec. IV C, Fig. 7. We understand this central result to be a clear indication of fractionalization, where the matter fermions scatter off gauge field degrees of freedom, with the latter acting as a thermally activated disorder. We note that on any finite system remnants of a DW will remain within the spectrum.

At very low temperatures, $T/J_z \lesssim 0.1$, the gauge excitations will start to freeze-out and the correlation function will approach the form of $C_{\mu\mu}(\omega)$ within the ground state sector, Fig. 7. This regime suffers from large finite size effects, and it is difficult to be tackled with our methods (see also the discussion in the context of Fig. 4).

The low-ω spectral hump in the correlation function displays a clearly visible, sharp dip as $\omega \to 0$, with $C(\omega \to 0) \simeq 0$, as can be read off from Fig. 2(b). This is particularly obvious at elevated temperatures. For semantic simplicity, we coin this suppression of the *regular* part of the conductivity spectrum, approaching zero only at the single point $\omega = 0$, a *pseudogap*. The behavior of this low frequency pseudogap with system size is crucial in order to characterize the system as conducting or insulating in the thermodynamic limit and requires a careful finite size analysis. Either the pseudogap will close as $L \to \infty$ and the system will have a conducting dc channel, or the pseudogap remains open. In the latter case the system will be characterized by the presence (absence) of a finite DW as an ideal conductor (insulator). These issues relate the system directly to questions of disorder in Dirac semimetals [67,68]. While our ED provides clear evidence for signatures of fractionalization in the dynamical correlation function, a convincing answer to the behavior of the pseudogap with system size requires larger lattices, which we will tackle with the average gauge configuration approach, presented in Sec. IV B.

Next, we focus on the temperature dependence of the ballistic contribution to the thermal conductivity, namely the DW, Eqs. (7) and (8). In Fig. 3, we present the temperature dependence of the DW for three different system sizes, acquired from the degeneracy plateau as usual [49]. The general form of the temperature dependence of the DW is that of a typical spin system exhibiting a maximum around $T \approx J_z$. With increasing system size, the magnitude of the DW is reduced. Note that this is different from the behavior of the DW

obtained for other transport quantities in Ref. [66]. Although the system sizes at hand do not allow for a safe finite size extrapolation, our findings are suggestive of a vanishing DW in the thermodynamic limit. This picture is further corroborated by the AGC method, presented in Sec. IV B [69].

B. Average gauge configuration (AGC)

In this section, we introduce an *approximate* method to evaluate the current correlation function, capturing the main physics, and allowing to reach systems of $\sim 60 \times 60$ sites, i.e., $\sim O(100)$ larger than with ED, which is crucial to understand the low frequency regime of the correlation function. The main idea is to reduce the full trace $Tr_\eta[\dots]$ to an average $\langle \dots \rangle_{n(T)}$ over only dominant gauge configurations, set by a temperature dependent *mean* density $n(T)$ of elementary gauge excitations off the gauge ground state. I.e., we reduce the evaluation of $C_{\mu\mu}(t)$ to a *disorder problem* in a system of free fermions with an emergent temperature dependent defect density

$$C_{\mu\mu}(t) \approx \langle \langle \mathcal{J}_\mu(t) \mathcal{J}_\mu \rangle_{d(\eta)} \rangle_{n(T)} . \tag{13}$$

Several comments are in order for this approach. First, while the Hamiltonian (2) and (3) is formulated in terms of matter fermions and gauge fields $\eta_{\mathbf{r}}$, the physical degrees of freedom are rather fermions and fluxes. In turn, depending on the temperature, fluctuations in $n(T)$ may be very large, rendering a mean field treatment in terms of the number of excited fluxes $\Phi(T)$ more appropriate. On the Kitaev ladder [59], this can be achieved by a direct mapping between $n(T)$ and $\Phi(T)$. On the honeycomb lattice this is not feasible. To make progress, we confine ourselves to temperatures above a scale T_R, which is elevated enough, such that a large number of fluxes is excited. Then, random gauge and flux ensembles will both behave similarly.

To approximate the scale T_R, we evaluate $n(T)$ and its fluctuations $\delta n(T)$, $\Phi(T)$, and its temperature derivative $\Phi'(T)$, as well as a thermodynamic observable, namely the specific heat C_V *exactly* on a finite system of $N = 6 \times 6$ sites. We use

$$n(T) = \frac{1}{ZN} \mathrm{Tr}_\eta Z_{d(\eta)} n_\eta , \tag{14}$$

where n_η is the number of gauge fields flipped off the uniform ground state sectors, excluding degenerate ground state sectors. The flux density is defined by

$$\Phi(T) = \frac{1}{ZN} \sum_{\{\eta_{\mathbf{r}}\}} Z_{d(\eta)} \sum_{\mathbf{r}} \Phi_{\mathbf{r}} , \quad \Phi_{\mathbf{r}} = \eta_{\mathbf{r}} \eta_{\mathbf{r}+\mathbf{e}_x-\mathbf{e}_y} . \tag{15}$$

First, Fig. 4(a) shows that at very low temperatures, $n(T)$ and $\Phi(T)$ represent the gauge homogeneous ground state. Second, at temperatures $T/J_z \sim 0.03$, well below the single gauge flip gap $\Delta_1/J_z \simeq 0.263$ [28], collective gauge excitations lead to a rapid increase of $n(T)$, a downturn of $\Phi(T)$, and a region of large fluctuations $\delta n(T) > n(T)$. Third, and for $T \gtrsim 0.1 J_z \equiv T_R$, the system has essentially settled into a *completely random* gauge state with its proper infinite temperature limiting value of $n_\infty \simeq 0.434$ for $N = 6 \times 6$ [70]. In this regime the system can be considered as free fermions scattering from a fully random binary potential.

In the crossover region $n(T) \sim 1/[e^{(\Delta/T)^b} + 1]$ with $\Delta = 0.06$, and $b = 3.5$ for the finite system [71]. This rather abrupt

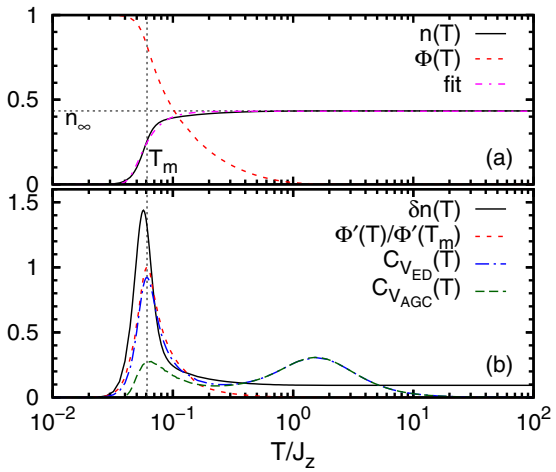

FIG. 4. (a) Temperature dependence of the mean density of gauge excitations $n(T)$ and the flux density $\Phi(T)$. A fit, $n(T) \sim 1/[e^{(\Delta/T)^b} + 1]$, is shown, with $\Delta = 0.06$, and $b = 3.5$. The infinite temperature limit of $n(T \to \infty) = n_\infty = 0.434$ is marked by a horizontal gray dashed line [70]. (b) Temperature dependence of the fluctuations of the mean density of gauge excitations $\delta n(T)$ and the derivative of the flux density $\Phi'(T)$ normalized to its minimum value at the crossover temperature $\Phi'(T_m) = -15.16$. Vertical dashed gray line: location of $T_m \simeq 0.06 J_z$. In addition, the specific heat is shown, obtained from ED and from the AGC methods, labeled accordingly. For the AGC, $n(T)$ as fitted to the ED result is used. All ED data from an $N = 6 \times 6$ sites system. The AGC data from an $N = 20 \times 20$ system, with $N_R = 20\,000$ realizations.

transition is likely due to gauge-gauge interactions and the large degree of degeneracy of the gauge fields for a given number of fluxes [72]. Considering the specific heat C_V [73] in Fig. 4(b), there is a clear release of entropy of the fluxes or the gauges in the vicinity of $T_m \simeq 0.06 J_z$ [66,74].

In view of $\delta n(T)/n(T)$ versus T, as in Figs. 4(a) and 4(b), the AGC will work acceptably well for $T \gtrsim T_R$. An indication of this is provided by evaluating C_V within the AGC, using $n(T)$ as from the ED, averaging over $N_R = 20\,000$ realizations, for a system with $N = 20 \times 20$. Obviously the agreement to the exact result is excellent down to $T \approx T_R$, below which the AGC does not account for all of the entropy release. To conclude: We confine all subsequent AGC calculations to $T_R \lesssim T < \infty$, using a fully random η ensemble, i.e., $n(T) = 0.5$.

In Fig. 5, we present the energy current correlation function obtained via the AGC method spanning three decades of temperature $T/J = 0.1, 2.1, 100$ and a binning of $\delta\omega = 0.001$. The left panels of the plot highlight the low frequency behavior of $C_{\mu\mu}(\omega, T)$ while the right ones scan the complete positive frequency range. First, the qualitative and quantitative agreement between the ED and the AGC method for all temperatures shown is remarkable [69]. At high temperatures there is a low frequency hump, the weight of which reduces with temperature due to the occupation numbers of the matter fermions. At the same time, and since the sum rule does not change with temperature, more weight is accumulated at high frequencies, as in Fig. 2.

The left panels of Fig. 5 show that apart from a smooth downturn at $\omega/J_z \approx 1$ there is a second, sharp dip structure

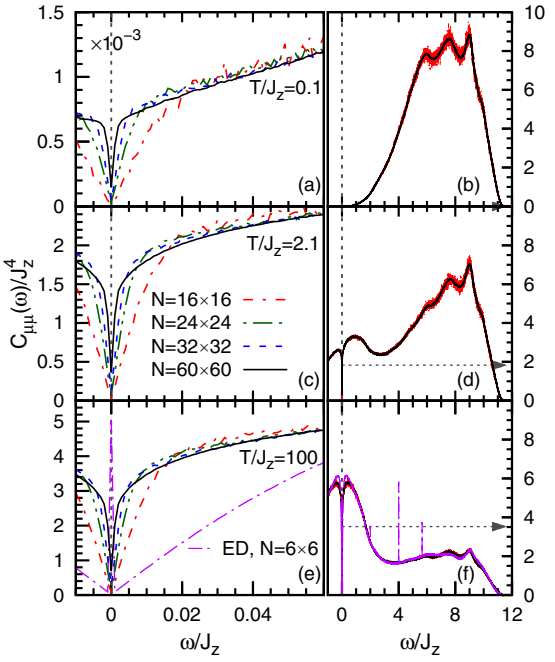

FIG. 5. $C_{\mu\mu}(\omega)$ obtained via the AGC method for various lattices $L = 16$–60 and three different temperatures $T/J_z = 0.1, 2.1, 100$ from top to bottom. The left panels show the low frequency behavior of $C_{\mu\mu}(\omega)$, emphasizing the development of the low frequency pseudogap with system size. The arrows in the right panels indicate the zero frequency extrapolation value from a second order polynomial. For $T/J_z = 100$ the ED results for a system with $L = 6$ are also displayed.

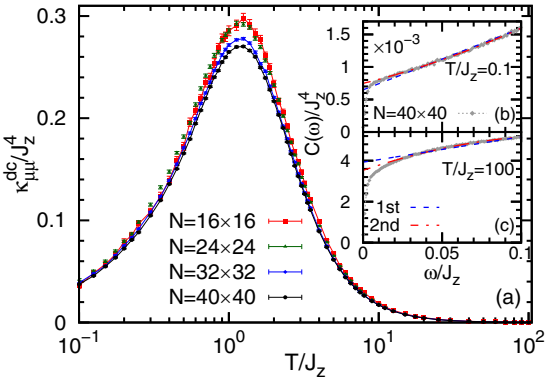

FIG. 6. (a) dc thermal conductivity $\kappa^{dc}_{\mu\mu}$ versus temperature for different system sizes, obtained from fitting a second order polynomial to the low frequency regime of the correlation function. In the insets (b) and (c) this low frequency behavior of $C(\omega)$ for a system of $L = 40$ at two temperatures $T/J_z = 0.1, 100$ is shown, as well as the corresponding linear and quadratic fit polynomials. The fitting range is restricted in the range $0.02 \leqslant \omega/J_z \leqslant 0.12$ for all the fits.

within a very low energy range of $\omega/J_z \ll 1$. This narrow part of the pseudogap displays a strong system size dependence, in stark contrast to the rest of the frequency spectrum, for which larger system sizes merely render the spectra smoother. It is interesting to note that the system sizes which can be reached by ED do not display this low frequency structure, Fig. 5(e), rendering the use of the AGC method essential [69]. This low-ω behavior with system size very much suggests the pseudogap to close in the thermodynamic limit. Therefore we extract a dc limit of the correlation function by fitting the data shortly before the dip. Because of the slight curvature within the data, we choose to fit a second order polynomial in the range [0.02–0.12], incorporating 100 frequency points, see also the inset of Fig. 6 and its discussion. The dc limit extrapolation for all three temperatures is marked by the gray arrows at the right panels of the plot. In addition, we note that we did not find any Drude weights for the systems analyzed [69]. In conclusion the system will be a normal dissipative conductor in the thermodynamic limit.

Next, in Fig. 6, we present the temperature dependence of the dc thermal conductivity, Eq. (5), for different system sizes. The overall behavior of $\kappa^{dc}_{\mu\mu}(T)$ versus T resembles that of other spin systems with, however, a low temperature increase with an exponent lower than one, a maximum related solely to an intrinsic energy scale, i.e., at $T/J_z \approx 1$, and lastly a $1/T^2$ decay at high temperatures. To assess this result several sources of uncertainty have to be mentioned. First, finite size effects are visible, which are however satisfyingly small. Second, choosing a particular fit function and fitting range induces an error. Its magnitude can be estimated from the two insets of Figs. 6(b) and 6(c), where either a first $(c_0 + c_1\omega)$ or a second order polynomial $(c_0 + c_1\omega + c_2\omega^2)$ is used, leading to slightly different dc extrapolations. Similar variations can be induced by changing the frequency window of the fit. In passing we mention that at high temperatures logarithmic fit functions, i.e., $\ln(c_0 + c_1\omega)$ also provide a good representation of $C(\omega \ll 1)$. Finally, the least square fit itself comprises an error which, however, is comparable with the size of the symbols depicted.

C. Fixed ground state gauge

As compared to the previous sections, fixing the gauge to a ground state configuration allows us to obtain analytic expressions for the conductivity. While in principle this only represents the limit $T/\Delta \to 0$, it can nevertheless be used to check the approach to low temperatures of the ED and AGC results. Moreover it is instructive to contrast a fictitious heat conductivity at *all* temperatures, arising from fixing the gauge to $\eta_{\mathbf{r}} = 1$ with that including the effects of thermally excited gauges. Since $\eta_{\mathbf{r}} = 1$ is a homogeneous state, we switch to momentum space, where the Hamiltonian and the current can be written as

$$H = \sum_{\mathbf{k}} \mathbf{D}^\dagger_{\mathbf{k}} h_{\mathbf{k}} \mathbf{D}_{\mathbf{k}}\,, \quad \mathcal{J}_\mu = \sum_{\mathbf{k}} \mathbf{D}^\dagger_{\mathbf{k}} L_{\mathbf{k},\mu} \mathbf{D}_{\mathbf{k}}\,, \tag{16}$$

where boldface $\mathbf{D}_{\mathbf{k}} = (d_{\mathbf{k}}, d^\dagger_{-\mathbf{k}})$ are 'spinors,' with $d^\dagger_{\mathbf{r}} = \sum_{\mathbf{k}} \exp(-i\mathbf{k}\cdot\mathbf{r}) d^\dagger_{\mathbf{k}}$. We label the two entries by light symbols $D_{\mathbf{k}\alpha}$, with $\alpha = 1,2$. Note that $D_{\mathbf{k}\alpha}$ are destruction (creation) operators depending on $\alpha = 1(2)$. Both, the Hamiltonian and current matrix elements, $h_{\mathbf{k}}$ and $L_{\mathbf{k},x(y)}$ for the $x(y)$ directions are encoded in 2×2 matrices. From Eqs. (2), (3), and (10) we get

$$h_{\mathbf{k}} = \begin{bmatrix} e_{\mathbf{k}} & i\Delta_{\mathbf{k}} \\ i\Delta_{-\mathbf{k}} & -e_{-\mathbf{k}} \end{bmatrix}, \quad L_{\mathbf{k},\mu} = l_{\mathbf{k},\mu} \begin{bmatrix} 1 & 1 \\ 1 & 1 \end{bmatrix} \tag{17}$$

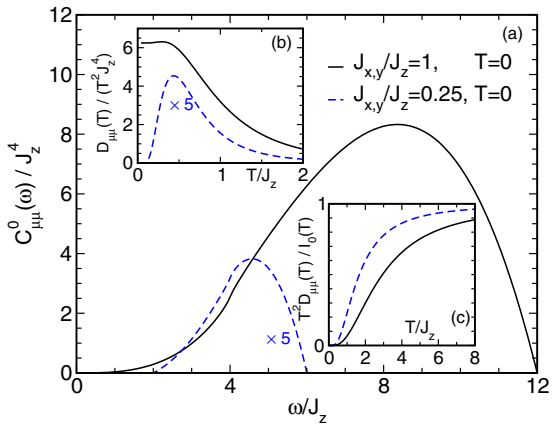

FIG. 7. (a) Black (blue) lines: $T=0$ regular part of dynamical current correlation function $C^0_{\mu\mu}(\omega)$ versus frequency $\omega>0$ using the ground state gauge for gapless(full) matter sector at $J_{x,y}/J_z = 1(0.25)$. Insets: (b) DW $D_{\mu\mu}/T^2$ versus temperature. (c) Ballistic weight $T^2 D_{\mu\mu}$ normalized to the weight of the regular part $I_0(T) = \int_{-\infty}^{\infty} C^0_{\mu\mu}(\omega)\, d\omega$.

where,

$$e_{\mathbf{k}} = 2[J_z - [J_x \cos(k_x) + J_y \cos(k_y)], \tag{18a}$$

$$\Delta_{\mathbf{k}} = 2[J_x \sin(k_x) + J_y \sin(k_y)], \tag{18b}$$

$$l_{\mathbf{k},\mu} = 2[J_\mu J_z \sin(k_\mu) - J_x J_y \sin(k_\mu - k_{\overline{\mu}})]\,, \tag{18c}$$

with $\overline{\mu} = y(x)$ for $\mu = x(y)$. After Bogoliubov transformation onto $h_{\mathbf{k}}$'s quasiparticle (QP) basis $c^{(\dagger)}_{\mathbf{k}}$, the Hamiltonian reads

$$H = \sum_{\mathbf{k}} \varepsilon_{\mathbf{k}} \left(c^\dagger_{\mathbf{k}} c_{\mathbf{k}} - \frac{1}{2} \right), \quad \text{with} \quad \varepsilon_{\mathbf{k}} = \sqrt{e^2_{\mathbf{k}} + \Delta^2_{\mathbf{k}}}\,. \tag{19}$$

Remarkably, the current operator is *invariant* under this Bogoliubov transformation. I.e., also in the QP basis $\mathcal{J}_\mu = \sum_{\mathbf{k}} \mathbf{C}^\dagger_{\mathbf{k}} L_{\mathbf{k},\mu} \mathbf{C}_{\mathbf{k}}$, with $L_{\mathbf{k},\mu}$ identical to Eq. (17) and $\mathbf{C}_{\mathbf{k}} = (c_{\mathbf{k}}, c^\dagger_{-\mathbf{k}})$. Since $L_{\mathbf{k},\mu}$ is not diagonal, the energy current has both QP and pairbreaking contributions. It is satisfying to realize that $2\, l_{\mathbf{k},\mu} = \varepsilon_{\mathbf{k}}\, \partial\varepsilon_{\mathbf{k}}/\partial k_\mu$. Therefore, and because of Eqs. (16) and (17), the naive expectation that the energy current can be written as

$$\mathcal{J}_\mu = \sum_{\mathbf{k}} \varepsilon_{\mathbf{k}} \frac{\partial \varepsilon_{\mathbf{k}}}{\partial k_\mu}\, c^\dagger_{\mathbf{k}} c_{\mathbf{k}} + \text{pair breaking terms} \tag{20}$$

is indeed satisfied by our definition of the local energy density Eq. (3).

Evaluating the current correlation function in the QP basis is straightforward. We get

$$C^0_{\mu\mu}(\omega) = \frac{2\pi}{N} \sum_{\mathbf{k}} \{2|l_{\mathbf{k},\mu}|^2 [\, 2 f_{\mathbf{k}}(1 - f_{\mathbf{k}})\, \delta(\omega) + f^2_{\mathbf{k}}\, \delta(\omega + 2\varepsilon_{\mathbf{k}}) + (1 - f_{\mathbf{k}})^2\, \delta(\omega - 2\varepsilon_{\mathbf{k}})]\}\,. \tag{21}$$

Where the superscript 0 refers to the ground state gauge, the term $\sim\delta(\omega)$ represents the DW, and the remaining two addends are the pair-breaking contributions.

Figure 7(a) shows $C^0_{\mu\mu}(\omega)$ for two representative cases of $J_{x,y}/J_z = 1$ ($J_{x,y}/J_z = 0.25$) referring to a gapless (gapped) matter sector. Several comments are in order. First, the regular spectrum at small ω reflects the gap structure of the low energy quasiparticle DOS combined with the energy current, leading to a power law $C^0_{\mu\mu}(\omega) \propto \omega^3$ in the gapless case, while displaying a linear onset above a finite gap. Second, within the spectrum a weak van-Hove singularity arises from the saddle point of the dispersion Eq. (19). E.g., for the gapless case in Fig. 7, there is a log-singular derivative of $C^0_{\mu\mu}(\omega)$ at $\omega = 4$, which is hardly noticeable on the scale of the plot. The inset Fig. 7(b) depicts the Drude weight divided by T^2 versus temperature. The main point is to demonstrate that in the gapless (gapped) case the Drude weight is *finite* for any $T > 0$ with $D_{\mu\mu} \propto T^2 (\propto \exp(-a/T))$ for $T \ll 1$. This implies that remaining within the ground state gauge, the system is a *ballistic* energy conductor, with infinite heat conductivity at any finite temperature. The inset of Fig. 7(c) details another aspect of the DW, namely that the spectral weight of the ballistic channel, i.e., $T^2 D_{\mu\mu}$, is of similar size to that of the integrated regular spectrum $I_0(T) = \int_{-\infty}^{\infty} C^0_{\mu\mu}(\omega)\, d\omega$.

V. DISCUSSION AND CONCLUSION

In conclusion, we have studied the dynamical longitudinal heat transport of the 2D Kitaev model on the honeycomb lattice. Our conclusions are based on three complementary approaches, using the mapping of the spin Hamiltonian onto matter fermions and a $\mathbb{Z}_2$ gauge field. First, we have employed numerically exact diagonalization of small systems, up to 72 spin sites. Second, to reach system sizes of up to 7200 spin sites, we have approximately restricted the complete gauge trace to only a random gauge configuration, demonstrating that this leads to reliable results over a wide range of temperatures. Finally, we have performed an analytical evaluation of transport properties in the uniform gauge sector.

Among our main findings is that fractionalization into Majorana matter and static gauge fields leaves a clear fingerprint on the spectrum of the current correlation function. In fact, thermally populated gauge excitations serve as an emergent disorder inducing an intrinsic energy scale for the relaxation of the matter fermion heat currents. This relaxation leads to a clearly observable low-ω accumulation of spectral weight in the current correlation function, increasing in intensity as the matter fermion density increases with temperature. We find this low-ω spectral weight to display a zero frequency pseudogap, which is strongly system size dependent. Based on finite size scaling, we have concluded that in the thermodynamic limit, the pseudogap closes, rendering the dc limit of the correlation function finite, albeit leaving a very sharp low-ω depletion within the spectrum behind. Therefore we have shown the 2D Kitaev model to be a normal dissipative heat conductor. This is in stark contrast to the Kitaev ladder, which is an insulator with a vanishing Drude weight and dc limit of the dynamical conductivity [59], as well as the one-dimensional Kitaev chain, which is a ballistic conductor [58] and features a finite Drude weight (DW). We find, that for the 2D Kitaev model, the DW is finite only on small systems or when gauge excitations are completely neglected.

We caution that our finite size analysis cannot exclude extreme scenarios, in which at system sizes way beyond our

reach, the pseudogap ceases to close and/or alters its variation with ω, such as to remain with a zero dc conductivity.

Our findings allow for a—certainly very coarse grained—comparative reference to magnetic thermal transport in 'conventional' 2D antiferromagnets (AFM) with magnon excitations and scattering from some form of extrinsic disorder or grain structures. Such transport has become of great interest, e.g., in the context of the parent compounds of the cuprate superconductors [4–8,75,76]. Straightforward power counting for this case yields $\kappa_{\text{magnon}} \sim T^2$ at low T, followed by a rapid drop beyond temperatures where the exponential decrease of the 2D magnetic correlation length dominates the magnon's mean free path instead of the defect scattering length [76–78]. A similar T^2 behavior is only observed in the absence of gauge fluctuations for the Kitaev model, namely in the DW of the ground state sector (Fig. 7), as a consequence of the Dirac cone dispersion at the isotropic point. Due to the intrinsic thermally activated disorder, $\kappa^{dc}_{\mu\mu}$ of Fig. 6 displays two striking differences if compared to the thermal transport in conventional 2D AFMs, as described above: (i) it features a maximum set to the scale of the exchange energy, while in 2D AFMs the location of this maximum is nonuniversally related to the interplay between the correlation and defect scattering lengths, and (ii) it features an increase with T with an approximate power less than unity within the low-T range depicted.

From a materials point of view, compounds potentially proximate to the Kitaev model display a heat transport, intricately intertwined with lattice degrees of freedom [21–23]. Furthermore, these materials order magnetically at low temperatures [42,79] due to non-Kitaev magnetic interactions [80,81]. The impact of such additional interactions can be manifold, e.g., fluxes may acquire dispersion, contributing to the heat flow, drag effects may occur, or fluxes and matter fermions may recombine eventually destroying fractionalization. Currently it seems most promising to consider transport at elevated T, involving higher energy excitations. Here, recent inelastic neutron scattering experiments [42] and the magnetic contribution to the specific heat [22,82,83] show signatures consistent with Majorana matter. We hope that this picture would be further corroborated by future heat transport data as depicted in Fig. 6.

Note added. Recently, we have become aware of a related work by J. Nasu *et al.* [84].

ACKNOWLEDGMENTS

We thank C. Hess, B. Büchner, M. Vojta, S. Rachel, and Y. Motome for fruitful comments. The work of W.B. has been supported in part by the DFG through SFB 1143, project A02 and the NSF under Grant No. NSF PHY11-25915. W.B. also acknowledges the kind hospitality of the PSM, Dresden.

APPENDIX A: DEGENERACIES

This appendix highlights the role of the degeneracies of the Kitaev model with respect to the observable considered, namely the heat current correlation function. First, we recapitulate that the spectrum of the Kitaev model is highly degenerate. This is due to the fact that a '*chain flip*,' i.e., inverting the sign of $\eta_{\mathbf{r}}$ located on *all* z links attached to any particular xy chain is a unitary transformation [29], leaving the fermionic spectrum invariant. We emphasize that this degeneracy is a physical property and unrelated to spurious states which arise in some of the mappings [28] from spins to fermions and $\mathbb{Z}_2$ fields for the Kitaev model. While only the case of open boundary conditions (OBCs) along the xy chains is considered in Ref. [29], the degeneracy remains in place using Eqs. (2) and (3) with PBCs on the torus and also for our square lattice geometry.

On any finite system of $N = L \times L$ sites, and restricting to even $L = 2k$ with $k \in \mathbb{N}$ hereafter, chain flips will render each gauge configuration 2^{L-1} fold degenerate. On these *finite* systems, the ground state is either within the manifold of $\eta_{\mathbf{r}} = 1\ \forall \mathbf{r}$ [28], the *homogeneous* sector, or in a homogeneous sector, except for one '*line flip*', i.e., with $\eta_{\mathbf{r}} = 1\ \forall \mathbf{r}$, except for a single ladder of z links with $\eta_{\mathbf{r}} = -1$. The energies $E_{e(o)}$

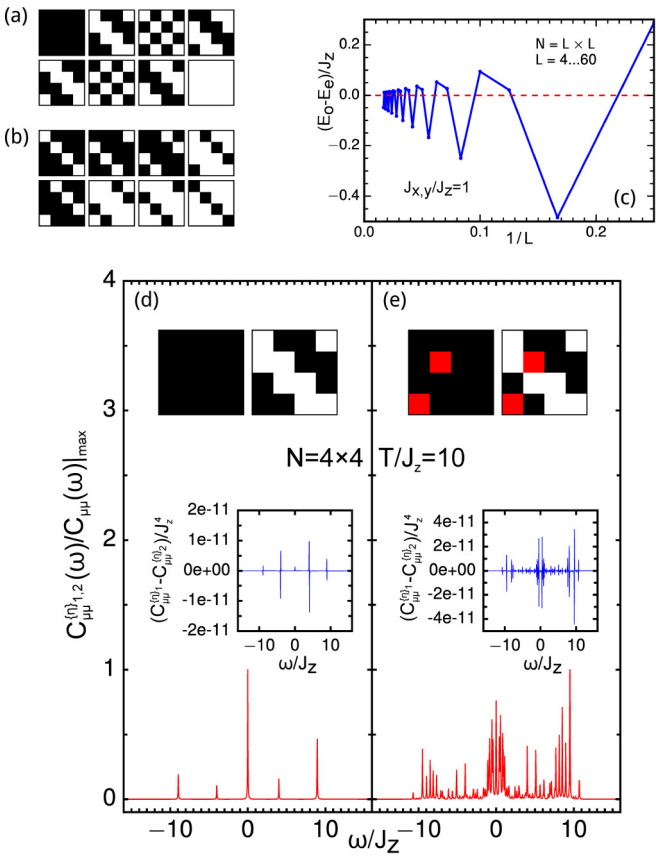

FIG. 8. (a),(b): All 2^{L-1} gauge amplitudes for the gauge sectors $\{\eta^0\}_{e,o}$ of the two lowest fermionic ground state energies E_e, E_o on a finite $L \times L = 4 \times 4$ square lattice with PBCs. (a) [(b)] exhibit an even [odd] number of line flips. Complete fermionic spectrum is degenerate within (a) [(b)], respectively. (c): Collapse of gauge sectors $\{\eta^0\}_{e,o}$ onto 2^L gauge sectors with degenerate fermionic spectrum, versus $1/L = 2k$, $k \in \mathbb{N}$ for $J_x = J_y = J_z$. $C_{\mu\mu}(\omega)$ on $L \times L = 4 \times 4$, at $T/J_z = 10$. (d) For two degenerate ground state gauge configurations $\{\eta\}_{1,2}$, shown in the graph, from the gauge sectors depicted in Fig. 8(a). Inset: proves conductivities identical up to numerical error. (e) For two fixed degenerate ground state gauge configurations $\{\eta\}_{1,2}$, shown in the graph, from the gauge sectors depicted in Fig. 8(a), including two flipped gauge fields as the red sites indicate. Inset: proves conductivities identical up to numerical error.

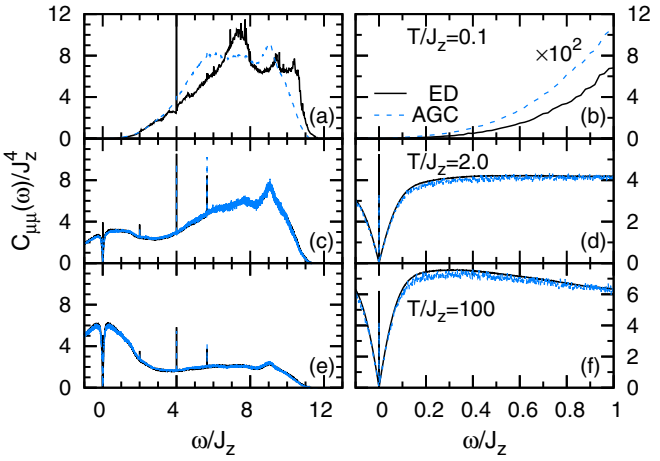

FIG. 9. Comparison of $C_{\mu\mu}(\omega)$ obtained via ED and AGC for a system of $N = 6 \times 6$ sites, with $J_x = J_y = J_z$, at three temperatures $T/J_z = 0.1, 2.0, 100$. The left panels display the full positive frequency spectrum of the correlation function at each temperature, while the right ones highlight the low frequency regime. The δ functions for the lowest temperature are binned in windows of $\delta\omega = 0.02$ while for the other two temperatures the bin size is $\delta\omega = 0.001$. The AGC data are averaged over $N_R = 50\,000$ random configurations with $n(T) = 0.5$.

of these two types of configurations are the two lowest of the system. For a 4×4 system these two gauge sectors are shown in Figs. 8(a) and 8(b). Figure 8(c) shows the collapse of the ground state energies for these two lowest energy sectors versus L. As $L \to \infty$ this implies a 2^L-fold degeneracy. Following the same logic, all energies of the model are at least 2^L-fold degenerate in the thermodynamic limit.

The main point of this appendix is to exemplify that not only the Hamiltonian but also the physical observable $C_{\mu\mu}(\omega)$ is invariant under chain-flip operations. In Figs. 8(d) and 8(e) we show this for two sets of degenerate gauge configurations on a 4×4 system. Figure 8(d) depicts $C_{\mu\mu}(\omega)$, using the first two gauge configurations from Fig. 8(a), while Fig. 8(e) employs the latter two gauges, with, however, gauge fields flipped on the two red sites. Obviously $C_{\mu\mu}(\omega)$ is identical within each of the two sets of gauges. Therefore, in the thermodynamic limit, the trace over η in Eq. (11) can in principle be restricted to one of the 2^L identical subtraces over gauge sectors, which are equivalent up to all chain-flip operations and a single line flip.

APPENDIX B: ED VS AGC FOR A SMALL SYSTEM

In this appendix we make a direct comparison of the ED, Sec. IV A, and the AGC, Sec. IV B, methods for a small system of $N = 6 \times 6$ sites. In Fig. 9, we plot the correlation function $C_{\mu\mu}(\omega)$, obtained via the ED and the AGC methods at three different temperatures $T/J_z = 0.1, 2, 100$ (from top to bottom). To anticipate finite size effects arising from the large mean level spacing of a system with a small linear dimension, we average over $N_R = 50\,000$ random configurations with $n(T) = 0.5$. At high temperatures and down to $T \approx J_z$, the agreement between the two methods is impressive. Not only is the overall behavior of $C_{\mu\mu}(\omega)$ *quantitatively* captured by the AGC method but also the fine structure yielded by singularities at the density of states. At the lowest temperature of $T = 0.1 J_z$, the AGC method clearly deviates from the exact high frequency structure of the correlation function, however the low frequency region $\omega < 4J_z$ is still captured rather well.

Figure 9 fortifies the physical conclusions extracted in the main text in the following two important aspects. First, it shows that the AGC method is capable of detecting the existence of a finite Drude weight (DW), although it fails to predict the correct weight of it. The latter does not come as a surprise since the evaluation of the DW involves only degenerate states and the AGC method is a random averaging approach. Therefore, the absence of any trace of a DW for the larger systems displayed in Fig. 5 shows that the DW decays fast with system size, and the weight of the ballistic channel completely disappears in the thermodynamic limit. Second, Fig. 9 provides additional support for the notion of a closing of the low frequency dip with system size extracted from the AGC. Namely, according to Fig. 5, ED displays only a very shallow pseudogap. However Fig. 9 proves that this is not at variance with the AGC but solely due to the smaller system size of ED, which in turn we have overcome by using the AGC method.

[1] J. E. Rives, G. S. Dixon, and D. Walton, J. Appl. Phys. **40**, 1555 (1969).
[2] F. W. Gorter, L. J. Noordermeer, A. R. Kop, and A. R. Miedema, Phys. Lett. A **29**, 331 (1969).
[3] H. N. De Lang, H. van Kempen, and P. Wyder, Phys. Rev. Lett. **39**, 467 (1977).
[4] Y. Nakamura, S. Uchida, T. Kimura, N. Motohira, K. Kishio, K. Kitazawa, T. Arima, and Y. Tokura, Phys. C (Amsterdam) **185-189**, 1409 (1991).
[5] C. Hess, B. Büchner, U. Ammerahl, L. Colonescu, F. Heidrich-Meisner, W. Brenig, and A. Revcolevschi, Phys. Rev. Lett. **90**, 197002 (2003).
[6] M. Hofmann, T. Lorenz, K. Berggold, M. Grüninger, A. Freimuth, G. S. Uhrig, and E. Brück, Phys. Rev. B **67**, 184502 (2003).
[7] X. F. Sun, J. Takeya, S. Komiya, and Y. Ando, Phys. Rev. B **67**, 104503 (2003).
[8] J.-Q. Yan, J.-S. Zhou, and J. B. Goodenough, Phys. Rev. B **68**, 104520 (2003).
[9] A. V. Sologubenko, K. Giannó, H. R. Ott, U. Ammerahl, and A. Revcolevschi, Phys. Rev. Lett. **84**, 2714 (2000).
[10] C. Hess, C. Baumann, U. Ammerahl, B. Büchner, F. Heidrich-Meisner, W. Brenig, and A. Revcolevschi, Phys. Rev. B **64**, 184305 (2001).
[11] A. V. Sologubenko, E. Felder, K. Giannò, H. R. Ott, A. Vietkine, and A. Revcolevschi, Phys. Rev. B **62**, R6108 (2000).
[12] A. V. Sologubenko, K. Giannò, H. R. Ott, A. Vietkine, and A. Revcolevschi, Phys. Rev. B **64**, 054412 (2001).
[13] C. Hess, H. ElHaes, A. Waske, B. Büchner, C. Sekar, G. Krabbes, F. Heidrich-Meisner, and W. Brenig, Phys. Rev. Lett. **98**, 027201 (2007).
[14] K. Takayuki, T. Nobuo, A. Tadashi, N. Takashi, K. Kazutaka, K. Norio, and K. Yoji, J. Phys. Soc. Jpn. **77**, 034607 (2008).
[15] N. Hlubek, P. Ribeiro, R. Saint-Martin, A. Revcolevschi, G.

Roth, G. Behr, B. Büchner, and C. Hess, Phys. Rev. B **81**, 020405(R) (2010).
[16] M. Yamashita, N. Nakata, Y. Senshu, M. Nagata, H. M. Yamamoto, R. Kato, T. Shibauchi, and Y. Matsuda, Science **328**, 1246 (2010).
[17] G. Kolland, O. Breunig, M. Valldor, M. Hiertz, J. Frielingsdorf, and T. Lorenz, Phys. Rev. B **86**, 060402(R) (2012).
[18] W. H. Toews, S. S. Zhang, K. A. Ross, H. A. Dabkowska, B. D. Gaulin, and R. W. Hill, Phys. Rev. Lett. **110**, 217209 (2013).
[19] S. J. Li, Z. Y. Zhao, C. Fan, B. Tong, F. B. Zhang, J. Shi, J. C. Wu, X. G. Liu, H. D. Zhou, X. Zhao, and X. F. Sun, Phys. Rev. B **92**, 094408 (2015).
[20] Y. Tokiwa, T. Yamashita, M. Udagawa, S. Kittaka, T. Sakakibara, D. Terazawa, Y. Shimoyama, T. Terashima, Y. Yasui, T. Shibauchi, and Y. Matsuda, Nat. Commun. **7**, 10807 (2016).
[21] I. A. Leahy, C. A. Pocs, P. E. Siegfried, D. Graf, S.-H. Do, K.-Y. Choi, B. Normand, and M. Lee, Phys. Rev. Lett. **118**, 187203 (2017).
[22] D. Hirobe, M. Sato, Y. Shiomi, H. Tanaka, and E. Saitoh, Phys. Rev. B **95**, 241112 (2017).
[23] R. Hentrich, A. U. B. Wolter, X. Zotos, W. Brenig, D. Nowak, A. Isaeva, T. Doert, A. Banerjee, P. Lampen-Kelley, D. G. Mandrus, S. E. Nagler, J. Sears, Y.-J. Kim, B. Büchner, and C. Hess, arXiv:1703.08623.
[24] G. Khaliullin, Prog. Theor. Phys. Suppl. **160**, 155 (2005).
[25] G. Jackeli and G. Khaliullin, Phys. Rev. Lett. **102**, 017205 (2009).
[26] J. Chaloupka, G. Jackeli, and G. Khaliullin, Phys. Rev. Lett. **105**, 027204 (2010).
[27] Z. Nussinov and J. van den Brink, Rev. Mod. Phys. **87**, 1 (2015).
[28] A. Kitaev, Ann. Phys. (NY) **321**, 2 (2006).
[29] X.-Y. Feng, G.-M. Zhang, and T. Xiang, Phys. Rev. Lett. **98**, 087204 (2007).
[30] H.-D. Chen and Z. Nussinov, J. Phys. A: Math. Theor. **41**, 075001 (2008).
[31] Z. Nussinov and G. Ortiz, Phys. Rev. B **79**, 214440 (2009).
[32] S. Mandal, R. Shankar and G. Baskaran, J. Phys. A: Math. Theor. **45**, 335304 (2012).
[33] A. Kitaev, Ann. Phys. (NY) **303**, 2 (2003).
[34] X.-G. Wen, Phys. Rev. B **40**, 7387 (1989).
[35] X.-G. Wen, Int. J. Mod. Phys. B **4**, 239 (1990).
[36] Y. Singh and P. Gegenwart, Phys. Rev. B **82**, 064412 (2010).
[37] Y. Singh, S. Manni, J. Reuther, T. Berlijn, R. Thomale, W. Ku, S. Trebst, and P. Gegenwart, Phys. Rev. Lett. **108**, 127203 (2012).
[38] K. W. Plumb, J. P. Clancy, L. J. Sandilands, V. V. Shankar, Y. F. Hu, K. S. Burch, H.-Y. Kee, and Y.-J. Kim, Phys. Rev. B **90**, 041112(R) (2014).
[39] K. A. Modic, T. E. Smidt, I. Kimchi, N. P. Breznay, A. Biffin, S. Choi, R. D. Johnson, R. Coldea, P. Watkins-Curry, G. T. McCandless, J. Y. Chan, F. Gandara, Z. Islam, A. Vishwanath, A. Shekhter, R. D. McDonald, and J. G. Analytis, Nat. Commun. **5**, 4203 (2014).
[40] T. Takayama, A. Kato, R. Dinnebier, J. Nuss, H. Kono, L. S. I. Veiga, G. Fabbris, D. Haskel, and H. Takagi, Phys. Rev. Lett. **114**, 077202 (2015).
[41] T. Dey, A. V. Mahajan, P. Khuntia, M. Baenitz, B. Koteswararao, and F. C. Chou, Phys. Rev. B **86**, 140405(R) (2012).
[42] A. Banerjee, C. A. Bridges, J. Q. Yan, A. A. Aczel, L. Li, M. B. Stone, G. E. Granroth, M. D. Lumsden, Y. Yiu, J. Knolle, S. Bhattacharjee, D. L. Kovrizhin, R. Moessner, D. A. Tennant, D. G. Mandrus, and S. E. Nagler, Nat. Mater. **15**, 733 (2016).
[43] A. Banerjee, J. Yan, J. Knolle, C. A. Bridges, M. B. Stone, M. D. Lumsden, D. G. Mandrus, D. A. Tennant, R. Moessner, and S. E. Nagler, Science **356**, 1055 (2017).
[44] M. Gohlke, R. Verresen, R. Moessner, and F. Pollmann, Phys. Rev. Lett. **119**, 157203 (2017).
[45] L. J. Sandilands, Y. Tian, K. W. Plumb, Y.-J. Kim, and K. S. Burch, Phys. Rev. Lett. **114**, 147201 (2015).
[46] J. Nasu, J. Knolle, D. L. Kovrizhin, Y. Motome, and R. Moessner, Nat. Phys. **12**, 912 (2016).
[47] S.-H. Baek, S.-H. Do, K.-Y. Choi, Y. S. Kwon, A. U. B. Wolter, S. Nishimoto, J. van den Brink, and B. Büchner, Phys. Rev. Lett. **119**, 037201 (2017).
[48] Y. Kasahara, K. Sugii, T. Ohnishi, M. Shimozawa, M. Yamashita, N. Kurita, H. Tanaka, J. Nasu, Y. Motome, T. Shibauchi, and Y. Matsuda, arXiv:1709.10286.
[49] F. Heidrich-Meisner, A. Honecker, and W. Brenig, Eur. Phys. J. Special Topics **151**, 135 (2007).
[50] C. Hess, Eur. Phys. J. Special Topics **151**, 73 (2007).
[51] B. S. Shastry and B. Sutherland, Phys. Rev. Lett. **65**, 243 (1990).
[52] X. Zotos, F. Naef, and P. Prelovšek, Phys. Rev. B **55**, 11029 (1997).
[53] A. Klümper and K. Sakai, J. Phys. A **35**, 2173 (2002).
[54] S. Fujimoto and N. Kawakami, Phys. Rev. Lett. **90**, 197202 (2003).
[55] F. Heidrich-Meisner, A. Honecker, D. C. Cabra, and W. Brenig, Phys. Rev. B **68**, 134436 (2003).
[56] T. Prosen, Phys. Rev. Lett. **106**, 217206 (2011).
[57] R. Steinigeweg, J. Gemmer, and W. Brenig, Phys. Rev. Lett. **112**, 120601 (2014).
[58] R. Steinigeweg and W. Brenig, Phys. Rev. B **93**, 214425 (2016).
[59] A. Metavitsiadis and W. Brenig, Phys. Rev. B **96**, 041115(R) (2017).
[60] D. Forster, *Hydrodynamic Fluctuations, Broken Symmetry, and Correlation Functions* (Benjamin, New York, 1975).
[61] J. V. Alvarez and C. Gros, Phys. Rev. Lett. **89**, 156603 (2002).
[62] X. Zotos, Phys. Rev. Lett. **92**, 067202 (2004).
[63] C. Psaroudaki and X. Zotos, J. Stat. Mech. (2016) 063103.
[64] J. Nasu, M. Udagawa, and Y. Motome, Phys. Rev. Lett. **113**, 197205 (2014).
[65] J. Nasu, M. Udagawa, and Y. Motome, J. Phys.: Conf. Ser. **592**, 012115 (2015).
[66] J. Nasu, M. Udagawa, and Y. Motome, Phys. Rev. B **92**, 115122 (2015).
[67] A. A. Nersesyan, A. M. Tsvelik, and F. Wenger, Nucl. Phys. B **438**, 561 (1995).
[68] E. McCann, K. Kechedzhi, V. I. Fal'ko, H. Suzuura, T. Ando, and B. L. Altshuler, Phys. Rev. Lett. **97**, 146805 (2006).
[69] See also Appendix B.
[70] At infinite temperature, $T \to \infty$, Eq. (14) leads to $n_\infty = \sum_{k=0}^{N} n_\eta(k)\binom{N}{k}/(N2^N)$, yielding $n_\infty \simeq 0.434$.
[71] In a free lattice gas picture where gauge flips are not interacting and they are gapped by $\Delta_1 \simeq 0.263 J_z$, one would expect $n(T) \sim 1/(\exp(\Delta_1/T)+1)$.
[72] See also Appendix A.
[73] The specific heat is evaluated via

$$C_V = \langle C_{Vd} \rangle + \left\langle E_m^2 \right\rangle - \langle E_m \rangle^2.$$

$E_m = \sum_i (\varepsilon_i^\eta - \frac{1}{2}) f_i$ is the thermal energy of the matter fermions in a particular $\{\eta\}$ configuration, and $C_{Vd} = \sum_i \varepsilon_i^{\eta 2} f_i(1 - f_i)$ their specific heat. Note that for only a single gauge field configuration, $C_V = C_{Vd}$, i.e., the two last terms in the above equation refer to the contributions to C_V from thermal gauge excitations.

[74] The release of entropy $S(T)$ of the fluxes, or the gauge field, respectively, can be readily seen from the qualitative agreement within the crossover region of the flux density temperature derivative with the specific heat $\Phi'(T) \propto C_V = T\partial S/\partial T$, Fig. 4(b), and a simple partial integration.

[75] A. S. T. Pires and L. S. Lima, Phys. Rev. B **79**, 064401 (2009).

[76] A. L. Chernyshev and W. Brenig, Phys. Rev. B **92**, 054409 (2015).

[77] S. Chakravarty, B. I. Halperin, and D. R. Nelson, Phys. Rev. B **39**, 2344 (1989).

[78] P. Hasenfratz, Eur. Phys. J. B **13**, 11 (2000).

[79] J. Chaloupka, G. Jackeli, and G. Khaliullin, Phys. Rev. Lett. **110**, 097204 (2013).

[80] L. Janssen, E. C. Andrade, and M. Vojta, Phys. Rev. B **96**, 064430 (2017).

[81] A. U. B. Wolter, L. T. Corredor, L. Janssen, K. Nenkov, S. Schönecker, S.-H. Do, K.-Y. Choi, R. Albrecht, J. Hunger, T. Doert, M. Vojta, and B. Büchner, Phys. Rev. B **96**, 041405 (2017).

[82] K. Mehlawat, A. Thamizhavel, and Y. Singh, Phys. Rev. B **95**, 144406 (2017).

[83] S.-H. Do, S.-Y. Park, J. Yoshitake, J. Nasu, Y. Motome, Y. S. Kwon, D. T. Adroja, D. J. Voneshen, K. Kim, T.-H. Jang, J.-H. Park, K.-Y. Choi, and S. Ji, arXiv:1703.01081.

[84] J. Nasu, J. Yoshitake, and Y. Motome, Phys. Rev. Lett. **119**, 127204 (2017).